ACS APPLIED MATERIALS & INTERFACES

Research Article

www.acsami.org

New Iridium Dopants forg White Phosphorescent Devices: Enhancement of Efficiency and Color Stability by an Energy-Harvesting Layer

Ho-Hsiu Chou, Yi-Kai Li, Yu-Han Chen, Ching-Chih Chang, Chuang-Yi Liao, and Chien-Hong Cheng*

Department of Chemistry, National Tsing Hua University, Hsinchu 30013, Taiwan

Supporting Information

ABSTRACT: A new light blue complex $(fmoppy)_2Ir(tfpypz)$ [bis(4′-fluoro-6′-methoxylphenyl pyridinato)-iridium(III)-3-(trifluoromethyl)-5-(pyridin-2-yl)-1,2,4-triazolate] and a new orange complex $(dpiq)_2Ir(acac)$ [bis(3,4-diphenylisoquinoline)-iridium(III)-acetylacetonate] were synthesized. These two complexes were used as the dopants for the fabrication of two-element white phosphorescent devices. Via the introduction of a thin energy-harvesting layer (EHL) to harvest the extra energy and exciton from the emission zone, highly efficient two-element white devices with excellent color stability were created. One of the best devices shows yellow-white color emission with an extremely high external quantum efficiency (EQE) of 21.5% and a current efficiency of 68.8 cd/A. The other device gave a pure white emission with an external quantum efficiency of 19.2% and a current efficiency of 53.2 cd/A. At a high brightness of 1000 cd/m^2, the EQE still remains as high as 18.9 and 17.2%. With a brightness of 1000−10000 cd/m^2, the CIE coordinates of these two devices shift by only (0.02, ≤0.01). The white phosphorescent devices with the EHL showed much higher efficiency and better color stability than the one without the EHL.

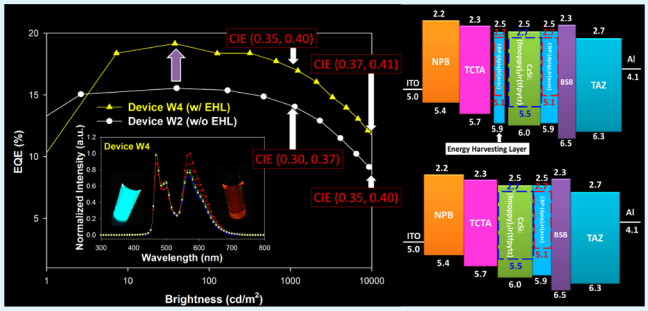

KEYWORDS: *WOLEDs, electroluminance, phosphorescent, low-efficiency roll-off, color stability*

1. INTRODUCTION

Recently, white organic light-emitting diodes (WOLEDs) have attracted a great deal of attention for their potential as a solid-state light source and as a back light unit for full-color display.[1−6] The major advantages of WOLEDs include high-resolution, flat-panel lighting without luminaries and flexibility for large-scale light sources.[7−10] For the purpose of lighting, WOLEDs are designed to give yellow-white emission to achieve high power efficiency. On the other hand, for the purpose of display, WOLEDs generally comprise three color elements to give nearly pure white emission.[11]

All phosphorescent WOLEDs have attracted researchers because of their intrinsic 4-fold higher efficiencies compared with those of fluorescent diodes.[9,12−18] The hybrid of different color emitters is a popular approach for fabricating two- or three-element WOLEDs. For a high-performance white emission device, the device should possess high external quantum efficiency (EQE), color stability, and low-efficiency roll-off. The control of the hole−electron carrier balance and recombination zone, the exciton confinement/blocking layer,[19−26] and the concentration of the chromophores[1−6] are the major approaches to creating high-performance white emission devices.

Although three-element WOLEDs can offer a better balanced white light in principle,[1−6] the use of three emitters with different wavelengths in a device can be a problem because of the interdopant energy transfer causing easily undesired emission in the production of the white color.[27−29] The low-image quality displays will be produced by the undesired color chromaticity and the poor batch-to-batch reproducibility.[28−30] WOLEDs with two emission layers were also frequently used. The device structure is simpler, and the fabrication is easier; however, some drawbacks are known. For example, as the applied voltage changes, the carrier recombination zone shifts, causing color variation at different voltages.[30] Thus, maintaining the color stability is a key issue for the two-element white light-emitting devices. To prevent the shift of the recombination zone and to stabilize the emission color, a buffer layer has been used in the device.[19,29] Nevertheless, the power efficiency decreases because of the influence of the hindered carriers.[31]

In this paper, we describe two-element white OLEDs as the hybrid of two new phosphorescent iridium complexes, a light blue $(fmoppy)_2Ir(tfpypz)$ complex and an orange $(dpiq)_2Ir(acac)$ complex. Both the light blue and orange light-emitting devices based on these two new iridium complexes as the dopants, respectively, show excellent efficiencies. In addition,

Received: March 27, 2013
Accepted: June 10, 2013
Published: June 10, 2013

the use of these two dopants and the introduction of an energy-harvesting layer (EHL) lead to all phosphorescence white electroluminescent devices with very high efficiencies, low-efficiency roll-off, and high color stability without using light out coupling.

2. EXPERIMENTAL SECTION

Physical Property Measurements. UV−vis absorption spectra were recorded using a Hitachi U-3300 spectrophotometer. PL spectra and phosphorescent spectra at 77 K were measured on a Hitachi F-4500 spectrophotometer. The electrochemical properties of the iridium complexes were measured by cyclic voltammetry (CV) using a Ag/Ag^+ (0.01 M $AgNO_3$) reference electrode (CH Instruments, Inc.). Nuclear magnetic resonance (NMR) spectra were measured in $CDCl_3$ on a Varian Inova 400 MHz FT-NMR spectrometer. The high-resolution mass spectrometry (HRMS) spectra were measured on a Finnigan/Thermo Quest MAT-95XL instrument. Elemental analysis was conducted with an Elementar Vario EL III instrument.

OLED Fabrication and Measurements.[32] Organic chemicals used for fabricating devices were generally purified by high-vacuum, gradient temperature sublimation. The EL devices were fabricated by vacuum deposition of the materials at 10^{-6} Torr onto a glass precoated with a layer of indium tin oxide with a sheet resistance of 25 Ω/square. The deposition rate for organic compounds is 1−2 Å/s. The Al/LiF cathode was deposited by evaporation of LiF with a deposition rate of 0.1 Å/s and then by evaporation of Al metal at a rate of 3 Å/s. The electron-transporting materials are TAZ [3-(4-biphenyl)-4-phenyl-5-(4-*tert*-butylphenyl)-1,2,4-triazole], BCP (bathocuproine), and Alq_3 [tris(8-hydroxyquinolinato)aluminum], while the hole-transporting layers contain NPB {4,4′-bis[*N*-(1-naphthyl)-*N*-phenylamino]-biphenyl} and TCTA [4,4′,4″-tris(*N*-carbazolyl)triphenylamine]. The effective area of the emitting diode is 9.00 mm^2. Current, voltage, and light intensity measurements were taken simultaneously using a Keithley 2400 source meter and a Newport 1835-C optical meter equipped with a Newport 818-ST silicon photodiode. Electroluminescence spectra were recorded on a Hitachi F-4500 fluorescence spectrophotometer.

Synthesis of Ligand fmoppy. Acetone (10 mL), 2-bromo-5-fluorophenol (1.1 mL, 10 mmol), and CH_3I (0.93 mL, 15 mmol) were added to a flask containing K_2CO_3 (2.4 g, 17 mmol). After the mixture had been stirred for 24 h at 40 °C, acetone was removed by rotary evaporator and the residue was extracted with ether. The organic layer was washed with anhydrous $MgSO_4$, and the solvent was removed under vacuum to give the desired pale yellow liquid, 1-bromo-4-fluoro-2-methoxybenzene. Then *n*-butyllithium (4.4 mL, 11 mmol, 2.5 M in hexane) was added dropwise to a stirred solution of 1-bromo-4-fluoro-2-methoxybenzene (2.1 g, 10 mmol) in anhydrous tetrahydrofuran (40 mL) at −78 °C under a nitrogen atmosphere. After the mixture had been stirred at −78 °C for 1 h, trimethoxylborate (2.2 mL, 20 mmol) was added, and the solution was further stirred for 12 h at room temperature. The reaction was quenched with NH_4Cl and then the mixture extracted with CH_2Cl_2. The organic layer was collected and concentrated under reduced pressure. The white solid 4-fluoro-2-methoxyphenylboronic acid was obtained in 91% yield. $Pd(PPh_3)_4$ (0.034 g, 0.030 mmol) was added to a solution containing 4-fluoro-2-methoxyphenylboronic acid (1.0 g, 6.0 mmol), 2-bromopyridine (0.63 mL, 6.6 mmol), and K_2CO_3 (14 mL, 1 M) in 22 mL of anhydrous THF under a nitrogen atmosphere. The mixture was then heated at 60 °C for 12 h. After the mixture had cooled to room temperature, the reaction was quenched with water and the aqueous phase was extracted with ethyl acetate. The organic extracts were dried ($MgSO_4$) and concentrated to give the desired compound fmoppy (63% yield). ^1H NMR (400 MHz, $CDCl_3$): δ 8.66 (d, J = 4.4 Hz, 1H), 7.76−7.72 (m, 2H), 7.68 (t, J = 7.6 Hz, 1H), 7.18 (t, J = 6.8 Hz, 1H), 6.76 (t, J = 8.4 Hz, 1H), 6.70 (dd, J = 11.0, 2.0 Hz, 1H), 3.83 (s, 3H). ^{13}C NMR (100 MHz, $CDCl_3$) : δ 164.9, 162.5, 158.0, 155.0, 149.2, 135.5, 132.1, 124.7, 121.5, 107.3, 99.2, 55.5. HRMS (EI, m/z): calcd for $C_{12}H_{10}FNO$ 203.0746, found M^+ 203.0753.

Synthesis of Ligand dpiq.[33,34] $NiBr_2$(dppe) (0.090 g, 0.15 mmol) and Zn (0.39 g, 6.0 mmol) were added to a sealed tube. After the tube had been filled with nitrogen, anhydrous CH_3CN (15 mL), *N*-*tert*-butyl 2-bromobenzaldimine (0.72 g, 3.0 mmol), and 1,2-diphenylethyne (0.53 g, 3.0 mmol) were further added to the system via syringes, and the mixture was stirred at 80 °C for 1.5 h. The mixture was cooled to room temperature, filtered through a Celite/silica pad, and washed with CH_2Cl_2. The filtrate was concentrated under reduced pressure. The residue was purified on a silica gel column by gradient elution with a mixture of *n*-hexane and ethyl acetate (9:1, v/v) to give white solid product dpiq in 70% yield. ^1H NMR (400 MHz, $CDCl_3$): δ 8.36 (s, 1H), 8.05−8.03 (m, 1H), 7.67−7.57 (m, 3H), 7.37−7.31 (m, 5H), 7.25−7.18 (m, 5H). ^{13}C NMR (100 MHz, $CDCl_3$): δ 151.7, 150.5, 140.6, 137.2, 135.9, 131.2, 130.7, 130.5, 130.2, 128.3, 127.6, 127.6, 127.3, 127.1, 126.9, 125.6. HRMS (EI, m/z): calcd for $C_{21}H_{15}N$ 281.1204, found M^+ 281.1200.

Synthesis of $(fmoppy)_2Ir(tfpypz)$. $IrCl_3 \cdot nH_2O$ (0.38 g, 1.0 mmol) and the cyclometalating ligand fmoppy (2.2 mmol) were added to a round-bottom flask containing a mixture of 2-ethoxyethanol and water (3:1, v/v, 16 mL). The mixture was then stirred under nitrogen at 100 °C for 24 h and cooled to room temperature. The precipitate that formed was filtered and washed with H_2O, methanol, ether, and *n*-hexane. The solid was dried in vacuum to give the corresponding cyclometaled Ir^{III}-μ-chloro-bridged dimer. To a 25 mL flask were added the dimer, K_2CO_3 (0.15 g, 1.1 mmol), tfpypz[35−39] (1.1 mmol), and 2-ethoxyethanol (5 mL). The mixture was stirred at 80 °C under a nitrogen atmosphere for 12 h. After cooling to room temperature, the mixture was filtered and the solid was collected and washed with methanol, ether, and *n*-hexane to give desired iridium complex $(fmoppy)_2Ir(tfpypz)$ in 56% yield. ^1H NMR (400 MHz, CD_2Cl_2): δ 8.71 (d, J = 8.4 Hz, 1H), 8.62 (d, J = 8.4 Hz, 1H), 7.75 (d, J = 4.0 Hz, 2H), 7.70−7.63 (m, 3H), 7.56−7.55 (m, 2H), 7.02−6.98 (m, 1H), 6.97 (s, 1H), 6.90 (t, J = 7.2 Hz, 1H), 6.84 (t, J = 7.2 Hz, 1H), 6.35 (dd, J = 8.8, 2.4 Hz, 1H), 6.32 (dd, J = 9.0, 2.4 Hz, 1H), 5.58 (dd, J = 8.4, 2.4 Hz, 1H), 5.53 (dd, J = 8.6, 2.4 Hz, 1H), 3.94 (s, 6H). HRMS (FAB, m/z): calcd for $C_{33}H_{23}F_5IrN_5O_2$ 809.1401, found M^+ 809.1405. Anal. Calcd for $C_{33}H_{23}F_5IrN_5O_2$: N, 8.66; C, 49.01; H, 2.87. Found: N, 8.63; C, 48.94; H, 2.90.

Synthesis of $(dpiq)_2Ir(acac)$. A procedure similar to that used for $(fmoppy)_2Ir(tfpypz)$ was employed for the synthesis of iridium complex $(dpiq)_2Ir(acac)$. The compound was obtained in 42% yield. ^1H NMR (400 MHz, $CDCl_3$): δ 9.38 (s, 2H), 7.90 (d, J = 7.2 Hz, 2H), 7.62−7.47 (m, 14H), 7.43 (d, J = 6.8 Hz, 2H), 6.50−6.46 (m, 2H), 6.36−6.28 (m, 6H), 5.24 (s, 1H), 1.84 (s, 6H). ^{13}C NMR (100 MHz, $CDCl_3$): δ 184.8, 158.1, 151.2, 147.9, 145.5, 137.1, 137.0, 132.9, 131.3, 130.4, 130.4, 129.5, 129.4, 128.3, 127.8, 127.5, 127.3, 126.8, 126.6, 125.4, 120.4, 100.5, 29.0. HRMS (FAB, m/z): calcd for $C_{47}H_{35}IrN_2O_2$ 852.2328, found M^+ 852.2332. Anal. Calcd for $C_{47}H_{35}IrN_2O_2$: N, 3.29; C, 66.26; H, 4.14. Found: N, 3.27; C, 65.70; H, 4.14.

X-ray Diffraction Studies. Single-crystal X-ray diffraction data were recorded on a Bruker SMART Apex charge-coupled device (CCD) diffractometer using Mo Kα radiation (λ = 0.71073 Å). The data were assessed using SMART. Empirical absorption corrections were performed with SAINT+. The structure was determined on a personal computer using SHELXTL and refined using full-matrix least squares. Crystallographic refinement parameters and ORTEP drawings with atomic labeling for the $(dpiq)_2Ir(acac)$ complex were summarized in the Supporting Information. The crystallographic data (excluding structure factors) have been deposited in the Cambridge Crystallographic Data Centre as entry CCDC-889166. These data can be obtained free of charge via http://www.ccdc.cam.ac.uk/data_request/cif or by emailing data_request@ccdc.cam.ac.uk or contacting The Cambridge Crystallographic Data Centre, 12, Union Road, Cambridge CB2 1EZ, U.K. (fax, +44 1223 336033).

3. RESULTS AND DISCUSSION

Synthesis and Characterization. The two iridium complexes $(fmoppy)_2Ir(tfpypz)$ and $(dpiq)_2Ir(acac)$ were synthesized using the procedures depicted in Schemes 1 and

Scheme 1. Synthesis of Ligand fmoppy and Iridium(III) Complex $(fmoppy)_2Ir(tfpypz)$

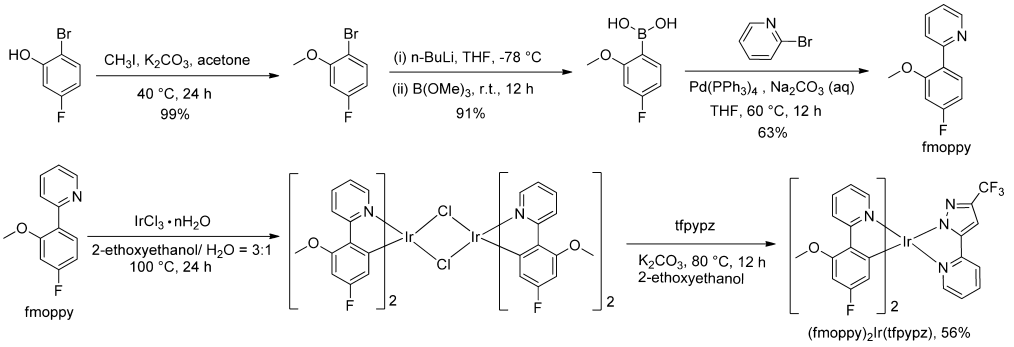

Scheme 2. Synthesis of dpiq and Iridium(III) Complex $(dpiq)_2Ir(acac)$

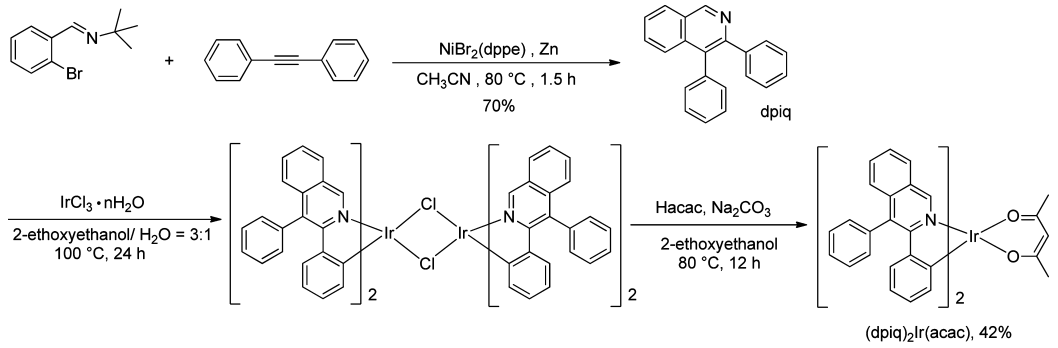

2, respectively. We synthesized the cyclometalating ligand fmoppy and the light blue light-emitting complex $(fmoppy)_2Ir(tfpypz)$ to see the effect of the methoxy moiety in fmoppy relative to a fluoro group on the emitting wavelength and lifetime of the corresponding iridium complexes. Complex $(dpiq)_2Ir(acac)$ in which the dpiq ligand with a phenyl at position 3 was designed and synthesized to determine the variation of the PL and molecular orbital levels relative to those of 1-phenylisoquinoline-based iridium complexes (see below). Ligand fmoppy was obtained from the Suzuki coupling of 4-fluoro-2-methoxyphenylboronic acid with 2-bromopyridine using a Pd(0) complex as the catalyst, while auxiliary ligand tfpypz[35−39] was prepared from the reaction of *o*-acetylpyridine with ethyl trifluoroacetate in the presence of NaH followed by condensation with hydrazine under acidic conditions. Similar to the synthesis of many other iridium complexes, the reaction of fmoppy with $IrCl_3 \cdot nH_2O$ gave chloride-bridged dimer $[Ir(fmoppy)_2Cl]_2$. Further treatment of the dimer with auxiliary ligand tfpypz afforded desired complex $(fmoppy)_2Ir(tfpypz)$ in 56% yield. As shown in Scheme 2, the dpiq ligand was synthesized in one step from the reaction of *N-tert*-butyl *o*-bromobenzaldehyde imine with diphenylacetylene using a nickel complex as the catalyst reported previously by us.[33,34] Orange iridium complex $(dpiq)_2Ir(acac)$ was prepared in two steps in a manner similar to the procedure for the preparation of $(fmoppy)_2Ir(tfpypz)$. The X-ray crystal structure of $(dpiq)_2Ir(acac)$ showed that the two chelated dpiq ligands are *cis* to each other with a *trans-N,N* and a *cis-C,C* configuration (see Figure 1 and the Supporting Information). The NMR spectra, element analysis, and mass spectral data of the two complexes are in agreement with the proposed structure.

Photophysical and Electrochemical Properties of the Iridium Complexes. Complex $(fmoppy)_2Ir(tfpypz)$ reveals

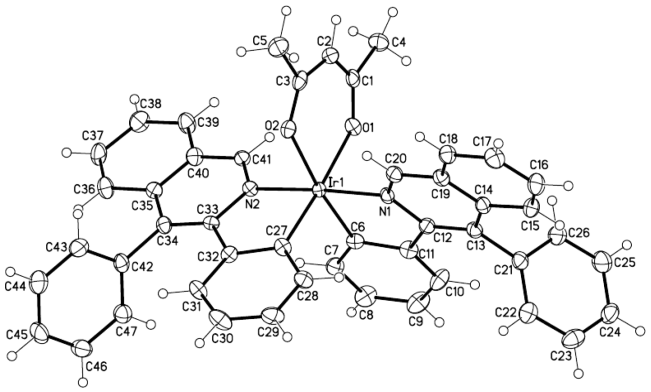

Figure 1. ORTEP diagram of $(dpiq)_2Ir(acac)$. Selected bond lengths (in angstroms): Ir(1)−C(27) = 1.978(4), Ir(1)−C(2) = 1.980(4), Ir(1)−N(1) = 2.019(3), Ir(1)−N(2) = 2.026(3), Ir(1)−O(1) = 2.152(3), and Ir(1)−O(2) = 2.172(3).

intense UV absorption bands between 260 and 330 nm (extinction coefficient ε of 20000−55000 M^{-1} cm^{-1}) attributed to spin-allowed $^1\pi-\pi^*$ transitions of the coordinated 2-phenylpyridine group and absorption bands between 350 and 400 nm (ε = 3000−10000 M^{-1} cm^{-1}) assigned to an interligand charge transfer (^{1}LLCT) and a metal-to-ligand charge transfer ($S_0 \rightarrow {}^1$MLCT).[40,41] The iridium complex also shows weak absorption bands above 400 nm (ε < 3000 M^{-1} cm^{-1}).[40,41] These absorptions are likely attributed to $S_0 \rightarrow {}^3$MLCT and $^3\pi-\pi^*$ transitions because of the strong spin-orbit coupling of the iridium complex. On the basis of the absorption edge of $(fmoppy)_2Ir(tfpypz)$ at 443 nm, the corresponding optical energy gap (E_g^{opt}) was calculated to be 2.85 eV.

The absorption spectrum of $(dpiq)_2Ir(acac)$ in dichloromethane is also shown in Figure 2. The absorption band between 290 and 390 nm (ε = 15000−65000 M^{-1} cm^{-1}) is

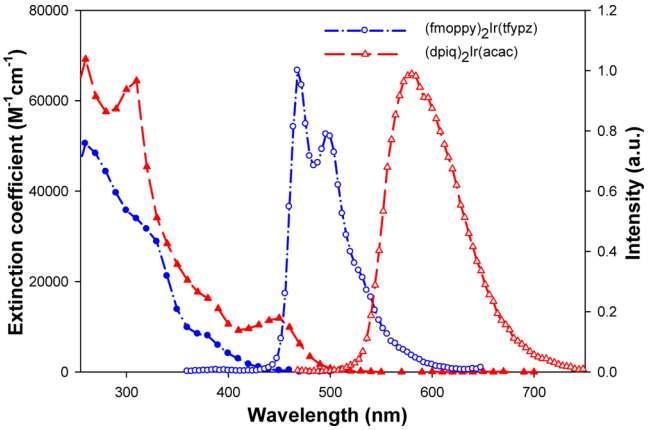

Figure 2. Absorption and emission spectra of $(fmoppy)_2Ir(tfpypz)$ and $(dpiq)_2Ir(acac)$ in dichloromethane.

assigned to the $^1\pi-\pi^*$ transition, while the absorptions in the region of 400−470 nm (ε = 3000−13000 M^{-1} cm^{-1}) are likely due to the ^{1}LLCT and $S_0 \rightarrow {}^1$MLCT transitions.[40,41] The weak absorptions above 470 nm (ε < 3000 M^{-1} cm^{-1}) are attributed to $S_0 \rightarrow {}^3$MLCT and $^3\pi-\pi^*$ transitions.[40,41] On the basis of the absorption edges of $(dpiq)_2Ir(acac)$ (506 nm), the corresponding E_g^{opt} were calculated to be 2.45 eV. The PL bands of $(fmoppy)_2Ir(tfpypz)$ and $(dpiq)_2Ir(acac)$ appear at 468 and 578 nm showing light blue and orange emission, respectively. Iridium complex $(dpiq)_2Ir(acac)$ with an extra phenyl group on the isoquinoline is red-shifted by ∼16 nm relative to the iridium complex without the phenyl substituent reported previously.[42] Compared with the previously reported blue emission iridium complexes $(dfpbpy)_2Ir(fppz)$[43] and FIrpytz [iridium(III) bis-(4,6-difluorophenylpyridinato)-4-(pyridin-2-yl)-1,2,3-triazolate],[44] the present $(fmoppy)_2Ir(tfpypz)$ shows a slightly longer emission wavelength because of the presence of the *ortho* methoxy group, which is less electron-withdrawing than a fluoro group. However, the emission wavelength of $(fmoppy)_2Ir(tfpypz)$ is almost the same as that of light blue iridium complex FIrpic {iridium(III) bis[(4,6-difluorophenyl)-pyridinato-*N*,$C^{2'}$]picolate}, which is widely used for the WOLEDs.[3,9,12]

CV measurements were employed to investigate the electrochemical properties of the complexes. The measurements were taken in dichloromethane solutions using tetrabutylammonium hexafluorophosphate ($TBAPF_6$) as the supporting electrolyte and ferrocene as the standard. The levels of the highest occupied molecular orbital (HOMO) of these two complexes are 5.53 and 5.10 eV for $(fmoppy)_2Ir(tfpypz)$ and $(dpiq)_2Ir(acac)$, respectively. These values were calculated from the oxidation potentials of the two iridium complexes, recorded relative to the ferrocence/ferrocenium (Fc/Fc^+) couple, of 0.73 and 0.30 V, respectively. The levels of the lowest unoccupied molecular orbital (LUMO) of the complexes were then estimated by subtracting the energy gap (E_g^{opt}) from the HOMO levels and are 2.68 and 2.65 eV, respectively. These results show that the HOMO and LUMO levels of $(fmoppy)_2Ir(tfpypz)$ are higher than those of the common blue iridium complexes,[43,44] because of the weaker electron-withdrawing ability of the methoxy group versus that of a fluoro atom or a cyano group. The phosphorescence quantum yields (PQYs) of $(fmoppy)_2Ir(tfpypz)$ and $(dpiq)_2Ir(acac)$ are 24.2 and 23.2%, respectively, measured in a degassed CH_2Cl_2 solution using cumarin (Φ = 0.99) as the standard. For reference, the PQY of blue dopant FIrpic was also measured to be 33.4%. In addition, the phosphorescence lifetimes of $(fmoppy)_2Ir(tfpypz)$ and $(dpiq)_2Ir(acac)$ were also measured and were 1.01 and 1.47 μs, respectively, in THF at room temperature at a concentration of 1 × 10^{-5} M. The photophysical and electrochemical properties are summarized in Table 1.

Performance of Blue and Orange OLEDs. To explore the ability of $(fmoppy)_2Ir(tfpypz)$ as a dopant emitter, two blue phosphorescence devices, B1 and B2, were fabricated. Device B1 consists of the following layers: ITO (indium tin oxide)/NPB (30 nm)/TCTA (20 nm)/CzSi: $(fmoppy)_2Ir(tfpypz)$ (8%) (25 nm)/TAZ (50 nm)/LiF (1 nm)/Al (100 nm), where NPB and TCTA are the hole-transporting materials (HTL), CzSi [9-(4-*tert*-butylphenyl)-3,6-bis(triphenylsilyl)-9*H*-carbazole] is the host,[45] and TAZ is the electron-transporting layer (ETL). The device reveals an external quantum efficiency (η_{ext}) of 11.6%, a current efficiency (η_c) of 19.9 cd/A, and Commission Internationale de L'Eclairage (CIE) coordinates of (0.13, 0.26). It is noteworthy that the blue light emitted from this device is deeper than that from the commonly used FIrpic-based light blue devices.[32,46] Nevertheless, device B1 showed a residual emission around 400 nm likely due to the high HOMO level of TAZ (6.3 eV)[32] that leads to injection the hole into the ETL. To remedy this leaking problem, we inserted a thin BSB layer[44] (4,4′-bis-triphenylsilanyl-biphenyl; HOMO = 6.5 eV) as a hole and exciton blocking layer between the CzSi and TAZ layers in device B2. The device consists of the following layers: ITO/NPB (30 nm)/TCTA (20 nm)/CzSi: $(fmoppy)_2Ir(tfpypz)$ (8%) (25 nm)/BSB (10 nm)/TAZ (40 nm)/LiF (1 nm)/Al (100 nm). As shown in Figures 3 and 4, the device shows an EL spectrum purely from the dopant with an external quantum efficiency of 18.7%, a current efficiency of 33.1 cd/A, a power efficiency of 22.7 lm/W, and CIE coordinates of (0.12, 0.27). At a brightness of 1000 cd/m^2, the external quantum efficiency still remains as high as 16.9%. We think that the insertion of BSB prevents the recombination of the hole and electron at the ETL and also leads to a better balance of the carriers and better confinement of the triplet excitons.

To understand the EL performance of $(dpiq)_2Ir(acac)$, device O1 was fabricated with the following multilayer

Table 1. Photophysical Properties and Electrochemical Properties of the Iridium Complexes

complex	absorption[a] λ (nm) [ε ($\times 10^3$ M^{-1} cm^{-1})]	emission[b] λ_{max} (nm)	HOMO/LUMO (eV)[c]	E_T (eV)[d]	τ (μs)[e]	Φ (%)[f]
$(fmoppy)_2Ir(tfpypz)$	264(54.3), 312(33.6), 377(8.3), 408(3.1)	468	5.53/2.68	2.65	1.01	24.2
$(dpiq)_2Ir(acac)$	307(65.7), 383(15.8), 448(12.1), 478(4.0)	578	5.10/2.65	2.15	1.47	23.2

[a]UV−vis absorption measured in CH_2Cl_2 at room temperature with ε and a solution concentration of 1 × 10^{-5} M. [b]Photoluminescence measured in CH_2Cl_2 at room temperature with a solution concentration of 1 × 10^{-4} M. [c]HOMO obtained from the oxidation potentials: LUMO = HOMO − E_g^{opt}. [d]Triplet energy gap. [e]Phosphorescence lifetimes measured in THF at room temperature at a solution concentration of 1 × 10^{-5} M. [f]Phosphorescence quantum yields measured in degassed CH_2Cl_2 relative to cumarin (Φ = 0.99).

dx.doi.org/10.1021/am401108m | ACS Appl. Mater. Interfaces 2013, 5, 6168−6175

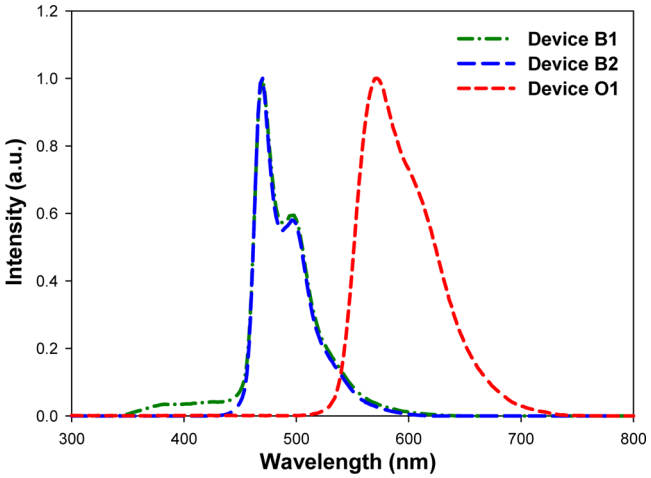

Figure 3. EL spectra of devices B1, B2, and O1.

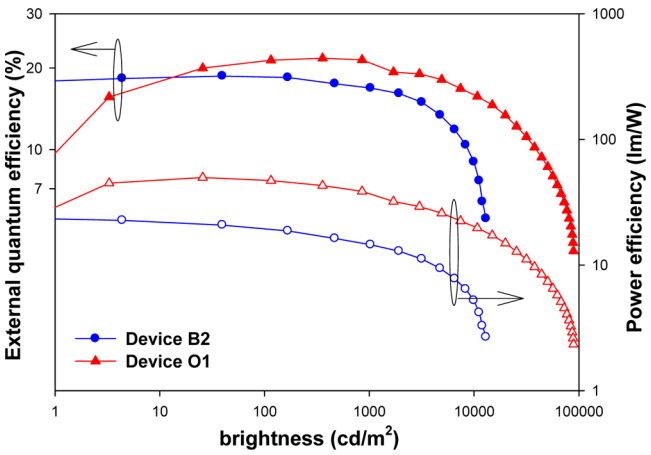

Figure 4. External quantum efficiency and power efficiency vs brightness of devices B2 and O1.

structure; ITO/NPB (10 nm)/TCTA (20 nm)/CBP: $(dpiq)_2Ir(acac)$ (3%) (30 nm)/BCP (10 nm)/Alq_3 (50 nm)/LiF (1 nm)/Al (100 nm), where CBP (4,4-*N*,*N*′-dicarbazole-biphenyl) is used as a host and BCP and Alq_3 are a hole blocking layer and ETL, respectively. The device exhibited an excellent external quantum efficiency of 21.6%, a current efficiency of 68.3 cd/A, a power efficiency of 49.7 lm/W, and a maximal brightness of 88877 cd/m^2 with CIE coordinates of (0.53, 0.47). At brightnesses of 1000 and 5000 cd/m^2, the external quantum efficiencies remain at 21.0 and 18.1%, respectively (see Figure 4). The performances of the present blue and orange light-emitting devices are comparable with the recently reported values.[47]

Performance of Two-Element WOLEDs. The EL spectra and the CIE coordinates of devices B2 and O1 indicate that the $(fmoppy)_2Ir(tfpypz)$- and $(dpiq)_2Ir(acac)$-based devices emit complementary wavelengths that are suitable for the fabrication of two-element WOLEDs. To control exciton formation in the blue emission region, $(fmoppy)_2Ir(tfpypz)$-based device B2 was used as the basic device structure and an orange light-emitting layer was inserted between the CzSi and BSB layers. For convenience, we call this type of device a type I device (see Figure 5). Device W1 with an ITO/NPB (30 nm)/TCTA (20 nm)/CzSi: $(fmoppy)_2Ir(tfpypz)$ (8%) (25 nm)/CBP: $(dpiq)_2Ir(acac)$ (3%) (5 nm)/BSB (10 nm)/TAZ (40 nm)/LiF (1 nm)/Al (100 nm) structure was thus fabricated. The device showed an external quantum efficiency of 14.5%, a current efficiency of 36.3 cd/A, a power efficiency of 27.8 lm/W, and CIE coordinates of (0.25, 0.34) to (0.31, 0.38) from 5 to 10 V (see Figure 6). The device appears to give less orange emission than expected. To improve the balance of the intensity of blue and orange emissions, we decreased the thickness of the blue light-emitting layer in the fabrication of device W2 with an ITO/NPB (30 nm)/TCTA (20 nm)/CzSi: $(fmoppy)_2Ir(tfpypz)$ (8%) (20 nm)/CBP: $(dpiq)_2Ir(acac)$ (3%) (10 nm)/BSB (10 nm)/TAZ (40 nm)/LiF (1 nm)/Al (100 nm) structure. As shown by the EL spectrum of this device in Figure 7, the orange emission grows relative to the blue emission at high voltages. However, its CIE coordinates changed from (0.30, 0.37) at 1000 cd/m^2 to (0.35, 0.40) at 10000 cd/m^2, shifted by (0.05, 0.03).

As shown in Table 2, the efficiencies and color stability of devices W1 and W2 appear to be only moderate. To further improve the performance of the device, we reduced the thickness of TCTA from 20 to 17 nm and added a 3 nm thick orange light-emitting layer between the TCTA and CzSi: $(fmoppy)_2Ir(tfpypz)$ layers hoping to harvest the extra energy and exciton from the blue emission layer. We call this extra layer the energy-harvesting layer (EHL) and this type of device a type II device (see Figure 5). Device W3 has an ITO/NPB (30 nm)/TCTA (17 nm)/CBP: $(dpiq)_2Ir(acac)$ (2%) (3 nm)/CzSi: $(fmoppy)_2Ir(tfpypz)$ (8%) (20 nm)/CBP: $(dpiq)_2Ir(acac)$ (3%) (10 nm)/BSB (10 nm)/TAZ (40 nm)/LiF (1 nm)/Al (100 nm) structure. We think that this 3 nm thick orange emission layer can provide two functions here. First, the layer can separate TCTA and the blue emission layer to prevent triplet exciton quenching by TCTA directly, because the triplet energy gap of TCTA (E_T = 2.7 eV)[32] is close to that of $(fmoppy)_2Ir(tfpypz)$ (E_T = 2.65 eV). Second, the layer can harvest the extra energy from the blue emission layer, resulting in the enhancement of device efficiency and color stability. In agreement with this expectation, device W3 revealed (see Figure 8) yellow-white light emission with an external quantum efficiency of 21.5%, a current efficiency of 68.8 cd/A, a power efficiency of 45 lm/W, and a maximal brightness of 34106 cd/m^2. At a high brightness of 1000 cd/m^2, the external quantum efficiency remains at 18.9% with a low roll-off value of 12.1%. At brightnesses from 1000 to 10000 cd/m^2, the CIE coordinates lie between (0.46, 0.45) and (0.44, 0.45), shifted by only (0.02, 0.00).

We continued to tune the concentration of $(dpiq)_2Ir(acac)$ to obtain a pure white emission. Device W4 was fabricated by reducing the concnetration of $(dpiq)_2Ir(acac)$ to 1%. Device W4 has an ITO/NPB (30 nm)/TCTA (17 nm)/CBP: $(dpiq)_2Ir(acac)$ (1%) (3 nm)/CzSi: $(fmoppy)_2Ir(tfpypz)$ (8%) (20 nm)/CBP: $(dpiq)_2Ir(acac)$ (3%) (10 nm)/BSB (10 nm)/TAZ (40 nm)/LiF (1 nm)/Al (100 nm) structure. As shown in Figure 9, a more balanced blue and orange emission with proper CIE coordination was achieved. No significant color variation at different brightnesses was observed for this device. At brightnesses from 1000 to 10000 cd/m^2, the CIE coordinates lie between (0.35, 0.40) and (0.37, 0.41), shifted only by (0.02, 0.01). Device W4 showed an external quantum efficiency of 19.2%, a current efficiency of 53.2 cd/A, a power efficiency of 32.1 lm/W, and a maximal brightness of 28780 cd/m^2. At a high brightness of 1000 cd/m^2, the external quantum efficiency remains at 17.2% with a low roll-off value of 10.4%.

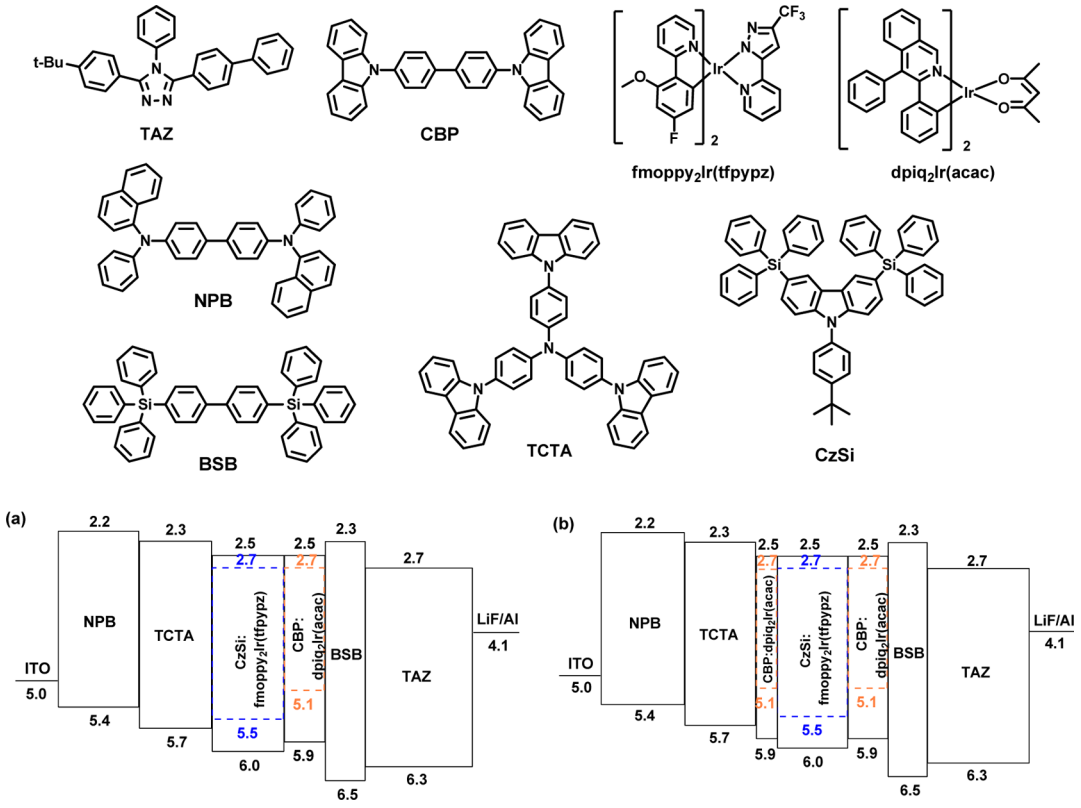

Figure 5. Chemical structures and HOMO and LUMO levels of the materials and the device structures used for (a) type I and (b) type II WOLEDs.

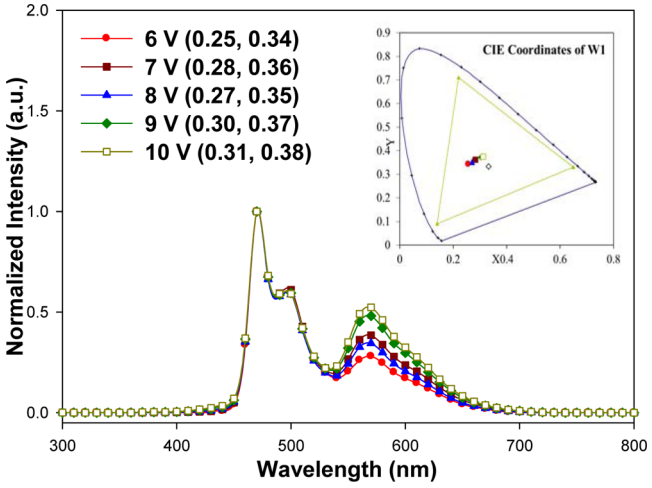

Figure 6. CIE coordinates and EL spectra of device W1.

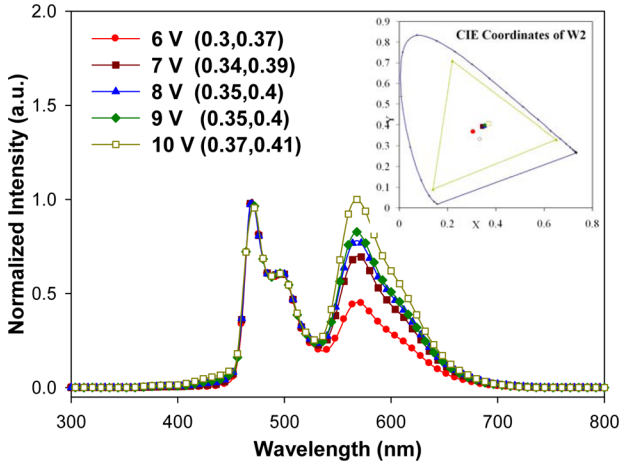

Figure 7. CIE coordinates and EL spectra of device W2.

We have successfully created two white light-emitting devices, a yellow-white device (W3) and a nearly pure white device (W4), by introducing the EHL and optimizing the concentration of the dopants. It appears that the performance of devices W3 and W4 with the EHL showed a much higher efficiency and better color stability than devices W1 and W2 without an EHL (Figure 10). The remarkable performance of W3 and W4 was attributed to the efficient exciton harvesting and confinement in the emission layers. Table 3 lists the EL performance of representative two-element WOLEDs recently reported in the literature.[26,32,47−56] Our white phosphorescent devices W3 and W4 using $(fmoppy)_2Ir(tfpypz)$ and $(dpiq)_2Ir(acac)$ as the light blue and orange color dopants, respectively, show excellent performance comparable to that of the most efficient devices reported.

4. CONCLUSIONS

We have successfully synthesized two new phosphorescent iridium complexes, $(fmoppy)_2Ir(tfpypz)$ and $(dpiq)_2Ir(acac)$, as the light blue and orange dopants, respectively. The $(fmoppy)_2Ir(tfpypz)$-based blue device achieves a high external quantum efficiency of 18.7% at CIE coordinates of (0.12, 0.27), while the orange $(dpiq)_2Ir(acac)$-based device exhibited a high external quantum efficiency of 21.6% at CIE coordinates of (0.53, 0.47). The latter is comparable to the best orange phosphorescent devices reported in the literature.[21] Moreover, we successfully utilized these two new complexes as the

dx.doi.org/10.1021/am401108m | ACS Appl. Mater. Interfaces 2013, 5, 6168−6175

Table 2. Performance of Devices B1, B2, O1, and W1−W4

device[a]	V_d[b] (V)	L_{max}[c] (cd/m^2, V)	η_{ext}[d] (%, V)	η_c[e] (cd/A, V)	η_p[f] (lm/W, V)	CIE (x, y) at 8 V
B1	3.7	8304, 13.5	11.6, 4.5	19.9, 4.5	14.3, 4.0	(0.13, 0.26)
B2	4.1	13024, 11.0	18.7, 5.0	33.1, 5.0	22.7, 4.5	(0.12, 0.27)
O1	3.1	88877, 16.5	21.6, 5.0	68.3, 5.0	49.7, 4.0	(0.53, 0.47)
W1	3.7	19505, 12.5	14.5, 4.5	36.3, 4.5	27.8, 4.0	(0.27, 0.35)
W2	3.7	26805, 13.0	15.5, 4.5	41.1, 4.5	31.3, 4.0	(0.35, 0.40)
W3	4.3	34106, 15.5	21.5, 5.5	68.8, 5.5	45.0, 4.5	(0.44, 0.45)
W4	4.5	28780, 16.5	19.2, 5.5	53.2, 5.5	32.1, 5.0	(0.35, 0.40)

[a]The cathode has an LiF (1)/Al (100) structure, and thicknesses are given in units of nanometers. Device B1 has an ITO/NPB (30)/TCTA (20)/CzSi: (fmoppy)$_2$Ir(tfpypz) (8%) (25)/TAZ (50) structure. Device B2 has an ITO/NPB (30)/TCTA (20)/CzSi: (fmoppy)$_2$Ir(tfpypz) (8%) (25)/BSB (10)/TAZ (40) structure. Device O1 has an ITO/NPB (10)/TCTA (20)/CBP: (dpiq)$_2$Ir(acac) (3%) (30)/BCP (10)/Alq$_3$ (50) structure. Device W1 has an ITO/NPB (30)/TCTA (20)/CzSi: (fmoppy)$_2$Ir(tfpypz) (8%) (25)/CBP: (dpiq)$_2$Ir(acac) (3%) (5)/BSB (10)/TAZ (40) structure. Device W2 has an NPB (30)/TCTA (20)/CzSi: (fmoppy)$_2$Ir(tfpypz) (8%) (20)/CBP: (dpiq)$_2$Ir(acac) (3%) (10)/BSB (10)/TAZ (40) structure. Devices W3 and W4 have an ITO/NPB (30)/TCTA (17)/CBP: (dpiq)$_2$Ir(acac) (x%) (3)/CzSi: (fmoppy)$_2$Ir(tfpypz) (8%) (20)/CBP: (dpiq)$_2$Ir(acac) (3%) (10)/BSB (10)/TAZ (40) structure (for W3, x = 2; for W4, x = 1). [b]Driving voltage. [c]Maximal brightness. [d]Maximal external quantum efficiency. [e]Maximal current efficiency. [f]Maximal power efficiency.

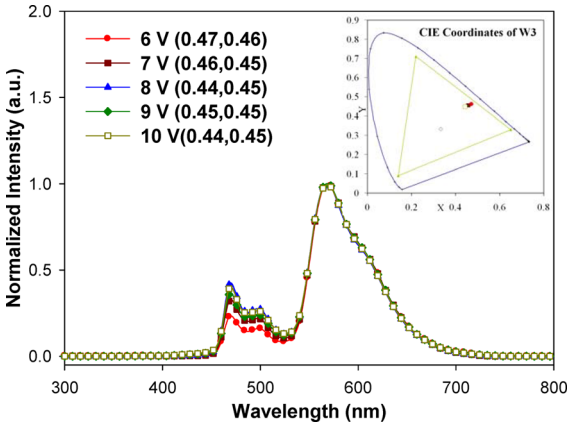

Figure 8. CIE coordinates and EL spectra of device W3.

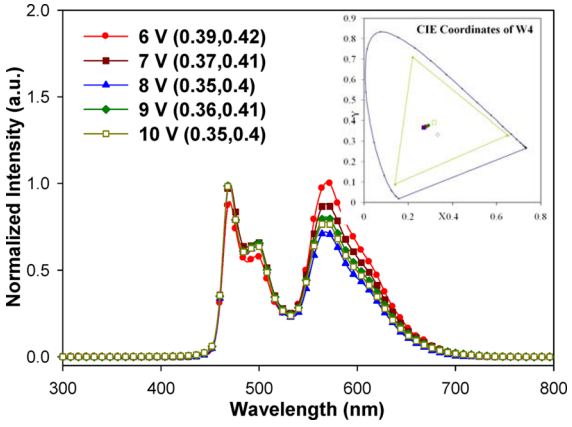

Figure 9. CIE coordinates and EL spectra of device W4 at different applied voltages.

dopants for the fabrication of WOLEDs. Via the introduction of an energy-harvesting layer in the white phosphorescent devices, we have achieved yellow-white and pure white light-emitting devices with EQE values of 21.5 and 19.2%, respectively. Both white phosphorescent devices showed better performances with low-efficiency roll-off and better color stability than those without the EHL. Compared with the previously reported results, this work has achieved one of the highest device efficiencies in WOLEDs.

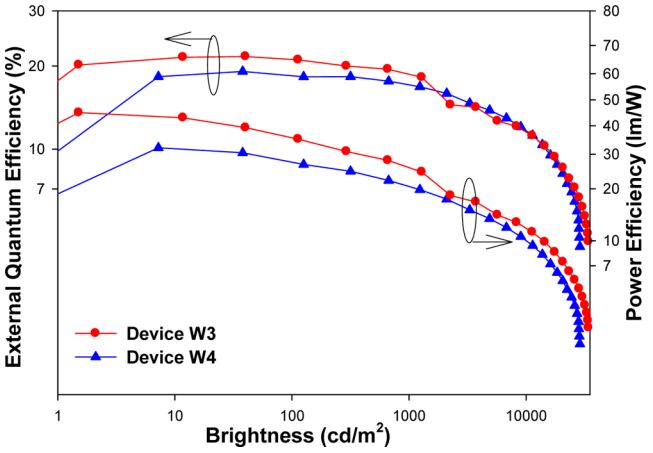

Figure 10. External quantum efficiency and power efficiency vs brightness of devices W3 and W4.

Table 3. EL Performance of Representative Two-Element WOLEDs

ref	η_{ext}[a] (%)	η_c[b] (cd/A)	η_p[c] (lm/W)	CIE (x, y)
26	19.3	52.8	42.5	(0.32, 0.38)
32	19.1	51.8	42.7	(0.37, 0.43)
50	26.2	68.6	34.0	(0.35, 0.44)
51	–	37.3	33.0	(0.38, 0.43)
52	–	25.1	–	(0.41, 0.41)
53	18.7	46.2	39.1	(0.39, 0.28)
54	18.8	30.3	–	–
55	21.5	60.1	38.1	(0.31, 0.50)
56	26.0	70.6	47.6	(0.38, 0.43)
this work	21.5	68.8	45.0	(0.44, 0.45)
this work	19.2	53.2	32.1	(0.35, 0.40)

[a]External quantum efficiency. [b]Current efficiency. [c]Power efficiency.

■ ASSOCIATED CONTENT

Supporting Information

X-ray crystallographic data file of complex (dpiq)$_2$Ir(acac). This material is available free of charge via the Internet at http://pubs.acs.org.

AUTHOR INFORMATION

Corresponding Author

*Telephone: +886 3 5715131. Fax: +886 3 5724698. E-mail: chcheng@mx.nthu.edu.tw.

Notes

The authors declare no competing financial interest.

ACKNOWLEDGMENTS

We thank the Ministry of Economic Affairs (100-EC-17-A-08-S1-042) and the National Science Council of the Republic of China (NSC-100-2119-M-007-010-MY3) for support of this research.

REFERENCES

(1) D'Andrade, B. W.; Forrest, S. R. *Adv. Mater.* **2004**, *16*, 1585−1595.
(2) Wang, Q.; Ma, D. *Chem. Soc. Rev.* **2010**, *39*, 2387−2398.
(3) D'Andrade, B. W.; Thompson, M. E.; Forrest, S. R. *Adv. Mater.* **2002**, *14*, 147−151.
(4) Mameno, K.; Nishikawa, R.; Suzuki, K.; Matsumoto, S.; Yamaguchi, T.; Yoneda, K.; Hamada, Y.; Kanno, H.; Nishio, Y.; Matsuoka, H.; Saito, Y.; Oima, S.; Mori, N.; Rajeswaran, G.; Mizukoshi, S.; Hatwar, T. K. In *Proceedings of IDW'02*; The Ninth International Display Workshops, Hiroshima, Japan; 2002; p 235.
(5) Burrows, P. E.; Gu, G.; Bulovic, V.; Shen, Z.; Forrest, S. R.; Thompson, M. E. *IEEE Trans. Electron Devices* **1997**, *44*, 1188−1203.
(6) Zhou, G.; Wong, W.-Y.; Suo, S. *J. Photochem. Photobiol., C* **2010**, *11*, 133−156.
(7) Kido, J.; Kimura, M.; Nagai, K. *Science* **1995**, *267*, 1332−1334.
(8) Sasabe, H.; Kido, J. *Chem. Mater.* **2011**, *23*, 621−630.
(9) Service, R. F. *Science* **2005**, *310*, 1762−1763.
(10) Su, S.-J.; Gonmori, E.; Sasabe, H.; Kido, J. *Adv. Mater.* **2008**, *20*, 4189−4194.
(11) Chen, S.; Tan, G.; Wong, W.-Y.; Kwok, H.-S. *Adv. Funct. Mater.* **2011**, *21*, 3785−3793.
(12) Lei, G.; Wang, L.; Qiu, Y. *Appl. Phys. Lett.* **2006**, *88*, 103508.
(13) Kim, S. H.; Jang, J.; Lee, J. Y. *Appl. Phys. Lett.* **2007**, *91*, 123509.
(14) Yook, K. S.; Jeon, S. O.; Joo, C. W.; Lee, J. Y. *Appl. Phys. Lett.* **2008**, *93*, 113301.
(15) Lee, M. T.; Lin, J.-S.; Chu, M.-T.; Tseng, M.-R. *Appl. Phys. Lett.* **2008**, *93*, 133306.
(16) Zhou, G.; Wong, W.-Y.; Yang, X. *Chem.—Asian J.* **2011**, *6*, 1706−1727.
(17) Wong, W.-Y.; Ho, C.-L. *Coord. Chem. Rev.* **2009**, *253*, 1709−1758.
(18) Wong, W.-Y.; Ho, C.-L. *J. Mater. Chem.* **2009**, *19*, 4457−4482.
(19) Tokito, S.; Iijima, T.; Tsuzuki, T.; Sato, F. *Appl. Phys. Lett.* **2003**, *83*, 2459−2461.
(20) Kim, C. H.; Shinar, J. *Appl. Phys. Lett.* **2002**, *80*, 2201−2203.
(21) Guo, F. W.; Ma, D. G.; Wang, L. X.; Jing, X. B.; Wang, F. S. *Semicond. Sci. Technol.* **2005**, *20*, 310.
(22) Yu, X.-Y.; Kwok, H.-S.; Wong, W.-Y.; Zhou, G.-J. *Chem. Mater.* **2006**, *18*, 5097−5103.
(23) Qin, D. S.; Tao, Y. *Appl. Phys. Lett.* **2005**, *86*, 113507.
(24) Seo, J. H.; Seo, J. H.; Park, J. H.; Kim, Y. K.; Kim, J. H.; Hyung, G. W.; Lee, K. H.; Yoon, S. S. *Appl. Phys. Lett.* **2007**, *90*, 203507.
(25) Huang, C. C.; Meng, H. F.; Ho, G. K.; Chen, C. H.; Hsu, C. S.; Huang, J. H.; Horng, S. F.; Chen, B. X.; Chen, L. C. *Appl. Phys. Lett.* **2004**, *84*, 1195−1197.
(26) Wang, Q.; Ding, J.; Ma, D. G.; Cheng, Y. X.; Wang, L. X.; Jing, X. B.; Wang, F. S. *Adv. Funct. Mater.* **2009**, *19*, 84−95.
(27) Thompson, M. E. EL 2006 Technical Digest; 2006; p 5.
(28) Ho, C.-L.; Lin, M.-F.; Wong, W.-Y.; Wong, W.-K.; Chen, C.-H. *Appl. Phys. Lett.* **2008**, *92*, 083301.
(29) Ho, C.-L.; Wong, W.-Y.; Wang, Q.; Ma, D. G.; Wang, L. X.; Lin, Z. Y. *Adv. Funct. Mater.* **2008**, *18*, 928−937.
(30) Jou, J. H.; Chiu, Y. S.; Wang, C. P.; Wang, R. Y.; Hu, H. C. *Appl. Phys. Lett.* **2006**, *88*, 193501.
(31) Chang, C.-H.; Chen, C.-C.; Wu, C.-C.; Chang, S.-Y.; Hung, J.-Y.; Chi, Y. *Org. Electron.* **2010**, *11*, 266−269.
(32) Chou, H.-H.; Cheng, C.-H. *Adv. Mater.* **2010**, *22*, 2468−2471.
(33) Korivi, R. P.; Cheng, C. H. *Org. Lett.* **2005**, *7*, 5179−5182.
(34) Shih, W.-C.; Teng, C.-C.; Parthasarathy, K.; Cheng, C.-H. *Chem.—Asian J.* **2012**, *7*, 306−313.
(35) Singh, S. P.; Kumar, D.; Jones, B. G.; Threadgill, M. D. *J. Fluorine Chem.* **1999**, *94*, 199−203.
(36) Fang, C.-H.; Chen, Y.-L.; Yang, C.-H.; Chi, Y.; Yeh, Y.-S.; Li, E. Y.; Cheng, Y.-M.; Hsu, C.-J.; Chou, P.-T.; Chen, C.-T. *Chem.—Eur. J.* **2007**, *13*, 2686−2694.
(37) Yeh, S.-J.; Wu, W.-C.; Chen, C.-T.; Song, Y.-H.; Chi, Y.; Ho, M.-H.; Hsu, S.-F.; Chen, C.-H. *Adv. Mater.* **2005**, *17*, 285−289.
(38) Song, Y.-H.; Chiu, Y.-C.; Chi, Y.; Cheng, Y.-M.; Lai, C.-H.; Chou, P.-T.; Wong, K.-T.; Tsai, M.-H.; Wu, C.-C. *Chem.—Eur. J.* **2008**, *14*, 5423−5434.
(39) Hsieh, C.-H.; Wu, F.-I.; Fan, C.-H.; Huang, M.-J.; Lu, K.-Y.; Chou, P.-Y.; Yang, Y.-H.; Wu, S.-H.; Chen, I.-C.; Chou, S.-H.; Wong, K.-T.; Cheng, C.-H. *Chem.—Eur. J.* **2011**, *17*, 9180−9187.
(40) Lamansky, S.; Djurovich, P.; Murphy, D.; Abdel-Razzaq, F.; Lee, H.-E.; Adachi, C.; Burrows, P. E.; Forrest, S. R.; Thompson, M. E. *J. Am. Chem. Soc.* **2001**, *123*, 4304−4312.
(41) Sajoto, T.; Djurovich, P. I.; Tamayo, A.; Yousufuddin, M.; Bau, R.; Thompson, M. E. *Inorg. Chem.* **2005**, *44*, 7992−8003.
(42) Li, C.-L.; Su, Y.-J.; Tao, Y.-T.; Chou, P.-T.; Chien, C.-H.; Cheng, C.-C.; Liu, R.-S. *Adv. Funct. Mater.* **2005**, *15*, 387−395.
(43) Chiu, Y.-C.; Chi, Y.; Hung, J.-Y.; Cheng, Y.-M.; Yu, Y.-C.; Chung, M.-W. *ACS Appl. Mater. Interfaces* **2009**, *1*, 433−442.
(44) Lin, J.-J.; Liao, W.-S.; Huang, H.-J.; Wu, F.-I.; Cheng, C.-H. *Adv. Funct. Mater.* **2008**, *18*, 485−491.
(45) Tsai, M. H.; Lin, H. W.; Su, H. C.; Ke, T. H.; Wu, C. C.; Fang, F. C.; Liao, Y. L.; Wong, K. T.; Wu, C. I. *Adv. Mater.* **2006**, *18*, 1216−1220.
(46) Chou, H.-H.; Shih, H.-H.; Cheng, C.-H. *J. Mater. Chem.* **2010**, *20*, 798−805.
(47) Gong, S.; Chen, Y.; Yang, C.; Zhong, C.; Qin, J.; Ma, D. *Adv. Mater.* **2010**, *22*, 5370−5373.
(48) Han, C.; Xie, G.; Xu, H.; Zhang, Z.; Xie, L.; Zhao, Y.; Liu, S.; Huang, W. *Adv. Mater.* **2011**, *23*, 2491−2496.
(49) Wu, H.; Zhou, G.; Zou, J.; Ho, C.-L.; Wong, W.-Y.; Yang, W.; Peng, J.; Cao, Y. *Adv. Mater.* **2009**, *21*, 4181−4184.
(50) Wang, R.; Liu, D.; Ren, H.; Zhang, T.; Yin, H.; Liu, G.; Li, J. *Adv. Mater.* **2011**, *23*, 2823−2827.
(51) Wang, Q.; Ding, J.; Ma, D.; Cheng, Y.; Wang, L. *Appl. Phys. Lett.* **2009**, *94*, 103503.
(52) Zhang, T.; Liu, M.; Li, T.; Ma, J.; Liu, D.; Xie, W.; Wu, C.-L.; Liu, S.-W.; Yeh, S.-C.; Chen, C.-T. *J. Phys. Chem. C* **2011**, *115*, 2428−2432.
(53) Sasabe, H.; Takamatsu, J.; Motoyama, T.; Watanabe, S.; Wagenblast, G.; Langer, N.; Molt, O.; Fuchs, E.; Lennartz, C.; Kido, J. *Adv. Mater.* **2010**, *22*, 5003−5007.
(54) Pérez-Bolívar, C.; Takizawa, S.; Nishimura, G.; Montes, V. A.; Anzenbacher, P., Jr. *Chem.—Eur. J.* **2011**, *17*, 9076−9082.
(55) Zou, J.; Wu, H.; Lam, C.-S.; Wang, C.; Zhu, J.; Zhong, C.; Hu, S.; Ho, C.-L.; Zhou, G.-J.; Wu, H.; Choy, W. C. H.; Peng, J.; Cao, Y.; Wong, W.-Y. *Adv. Mater.* **2011**, *23*, 2976−2980.
(56) Zhang, B.; Tan, G.; Lam, C.-S.; Yao, B.; Ho, C.-L.; Liu, L.; Xie, Z.; Wong, W.-Y.; Ding, J.; Wang, L. *Adv. Mater.* **2012**, *24*, 1873−1877.